Title

Therapeutic targeting of argininosuccinate synthase 1 (ASS1)-deficient pulmonary fibrosis

Journal

Molecular Therapy, 29(4)

ISSN

1525-0016

Authors

Li, Ji-Min
Yang, David C
Oldham, Justin
et al.

Publication Date

2021-04-01

DOI

10.1016/j.ymthe.2021.01.028

Peer reviewed

Molecular Therapy
Original Article

Therapeutic targeting of argininosuccinate synthase 1 (ASS1)-deficient pulmonary fibrosis

Ji-Min Li,[1,2] David C. Yang,[1,2] Justin Oldham,[1] Angela Linderholm,[1] Jun Zhang,[1,2] Jun Liu,[1,2] Nicholas J. Kenyon,[1] and Ching-Hsien Chen[1,2]

[1]Division of Pulmonary and Critical Care Medicine, Department of Internal Medicine, University of California, Davis, Davis, CA, USA; [2]Division of Nephrology, Department of Internal Medicine, University of California, Davis, Davis, CA 95616, USA

Argininosuccinate synthase 1 (ASS1) serves as a critical enzyme in arginine biosynthesis; however, its role in interstitial lung diseases, particularly idiopathic pulmonary fibrosis (IPF), remains largely unknown. This study aims at characterization and targeting of ASS1 deficiency in pulmonary fibrosis. We find that ASS1 was significantly decreased and inversely correlated with fibrotic status. Transcriptional downregulation of ASS1 was noted in fibroblastic foci of primary lung fibroblasts isolated from IPF patients. Genetic manipulations of ASS1 studies confirm that ASS1 expression inhibited fibroblast cell proliferation, migration, and invasion. We further show that the hepatocyte growth factor receptor (Met) receptor was activated and acted upstream of the Src-STAT3 axis signaling in ASS1-knockdown fibroblasts. Interestingly, both arginine-free conditions and arginine deiminase treatment were demonstrated to kill fibrotic fibroblasts, attenuated bleomycin-induced pulmonary fibrosis in mice, as well as synergistically increased nintedanib efficacy. Our data suggest ASS1 deficiency as a druggable target and also provide a unique therapeutic strategy against pulmonary fibrosis.

INTRODUCTION

Idiopathic pulmonary fibrosis (IPF) is one of the most frequent interstitial lung diseases (ILDs), and its incidence is increasing worldwide. This disease exhibits a median survival of less than 5 years from the time of diagnosis, as effective treatment is still limited.[1–4] The two US Food and Drug Administration (FDA)-approved therapeutic agents, nintedanib and pirfenidone, have recently entered clinical use. Nintedanib, a potent multi-kinase inhibitor targeting receptor tyrosine kinases (RTKs) in fibroblasts,[5,6] has been utilized as a standard antifibrotic for treatment of PF, but adverse effects are common with nintedanib therapy and worsen with a higher dose, resulting in drug discontinuation.[7,8] Of most concern, both nintedanib and pirfenidone are limited in therapeutic efficacy, as they only improve the lung function in patients, with little to no effect on overall mortality.[2,9,10] For these reasons, there is an urgent need to develop novel and viable therapeutic strategies for those diagnosed with IPF.

Lesions in IPF are dominated by excessive extracellular matrix (ECM) proteins and accumulation of active (aggressive) fibroblasts, displaying pathological alterations in cell proliferation, invasion, and differentiation.[11,12] These aggressive cells form foci and display enhanced ECM production and deposition, disturbing the alveolar architecture.[13,14] In recent years, RTKs have emerged as a major modulator of fibroblast activities and disease progression.[15] The hepatocyte growth factor (HGF) receptor (HGFR, or Met), an oncogenic RTK, has been recently demonstrated to participate in driving profibrotic phenotypes and contributing to PF.[16,17] Activation of Met signaling initiates phosphatidylinositol 3-kinase (PI3K)/AKT, mitogen-activated protein kinase (MAPK)/extracellular signal-regulated kinase (ERK), Src/STAT3 cascades that control cell growth, invasion, and migration during oncogenesis.[18] Despite extensive studies of the Met pathway in a broad range of malignancies, how Met activity is regulated in fibroblasts and its functional consequence in PF remain to be established.

Beyond dysregulated cell signaling, disruption of metabolic pathways has been recognized as a driver for many respiratory diseases, and metabolic reprogramming, including altered levels of metabolic enzymes and metabolites, is also noted in IPF.[19–22] Through integrated analysis of metabolomics data gathered from tissues isolated from PF patients[21,22] and transcriptomics from gene-expression datasets of PF tissues,[23] we noticed dysregulated expression of the metabolic enzyme argininosuccinate synthase 1 (ASS1) in fibrotic disorders. ASS1 is a rate-limiting enzyme responsible for biosynthesis of the semi-essential amino acid arginine in the urea cycle.[24] The role of ASS1 had been reported as a tumor suppressor, and a lack of ASS1 in cancers was found to induce arginine auxotrophy.[25–27] However, the expression of ASS1 and its contribution in lung diseases remain vastly unknown. In this study, we characterized the role of ASS1 in fibroblasts and tested the therapeutic potential of arginine starvation in lung fibrosis.

RESULTS

Downregulation of ASS1 occurs in fibrotic lung tissues and fibroblasts

Recent studies have characterized that altered metabolites and dysregulated metabolic pathways may contribute to several respiratory

Received 24 July 2020; accepted 19 January 2021;
https://doi.org/10.1016/j.ymthe.2021.01.028.

Correspondence: Ching-Hsien Chen, PhD, Department of Internal Medicine, University of California, Davis, 451 East Health Sciences Drive, GBSF 6311, Davis, CA 95616, USA.
E-mail: jchchen@ucdavis.edu

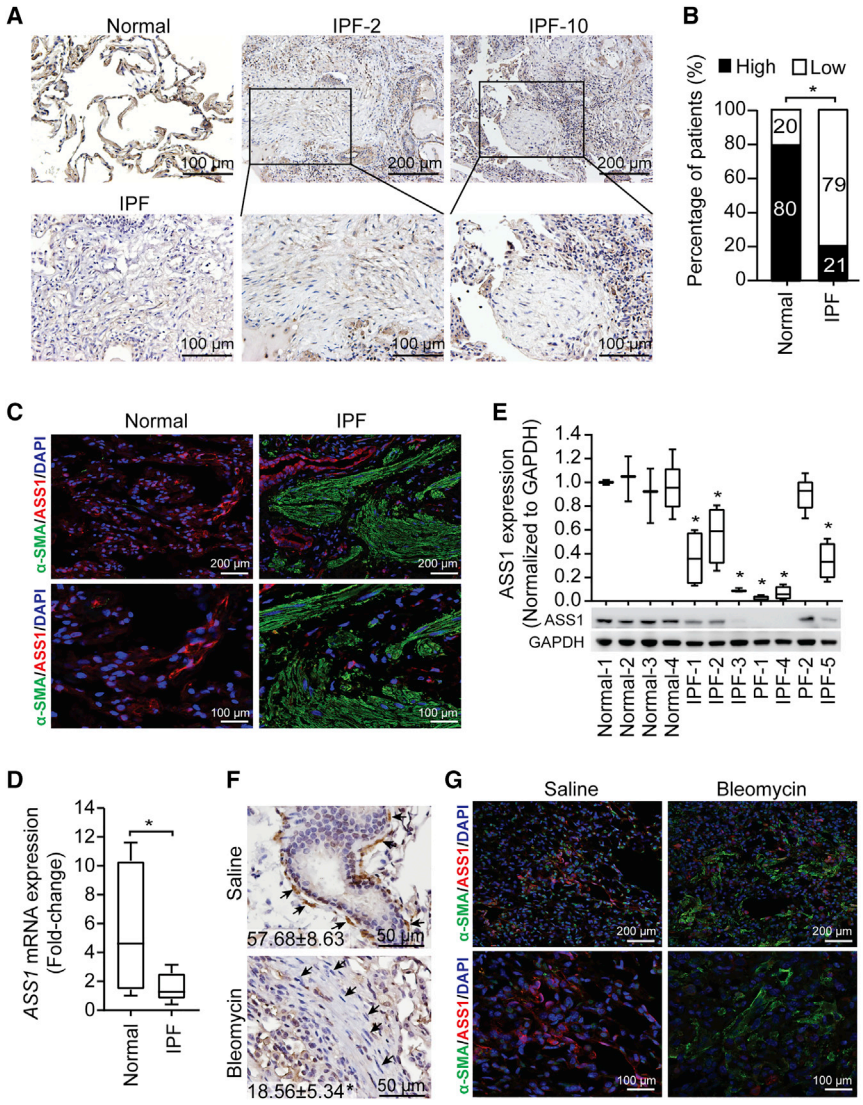

Figure 1. Aberrant downregulation of ASS1 in IPF lung tissues and fibroblasts

(A) Representative images of immunohistochemical staining using anti-ASS1 antibody in normal lung tissue (top left panel, n = 30) and IPF specimens from patients (bottom left panel, n = 14). IPF-2 (middle panel) and IPF-10 (right panel) are representative patients. Higher magnification images of boxed areas are shown below. (B) Percentage of patients with high and low levels of ASS1 expression corresponding to normal and IPF. Numbers in bars represent the percentage of patients for each condition. *p < 0.05. (C) Representative images of immunofluorescent staining of ASS1 (red color) and α-SMA (green color) in normal lung tissues and IPF specimens from patients. DAPI (blue color) is indicated as the nucleus. (D) Expression of ASS1 mRNA in primary normal fibroblasts and primary IPF fibroblast cells, as measured by qRT-PCR (n = 4; *p < 0.05 versus normal). (E) Immunoblotting analysis of ASS1 expression in 4 human primary normal fibroblasts (normal-1, -2, -3, and -4) and 7 fibroblast cells isolated from IPF and PF patients (IPF-1, -2, -3, -4, and -5 and PF-1 and -2). ASS1 expression was quantified using ImageJ software (n = 5; *p < 0.05 versus normal-1). (F) The levels of ASS1 were examined using immunohistochemical staining in lung tissue specimens from saline- and bleomycin (BLM)-exposed mice. Arrows, fibroblast cells. Numbers, the percentage of ASS1-positive fibroblast cells was quantified by ImageJ software. Data are expressed as mean ± SE. *p < 0.05. (G) Representative images from immunofluorescent staining with anti-ASS1 antibody (red color) and anti-α-SMA antibody (green color) in lung tissues of mice exposed to either saline or BLM. DAPI (blue color) is represented as the nucleus.

diseases, including PF.[19–22] To profile the metabolic pathways altered between normal and IPF cells, we conducted metabolomic studies of primary lung fibroblasts derived from healthy donors ($n = 6$) and PF patients ($n = 10$), as we reported previously.[28] Metabolite set enrichment analysis (MSEA) identified the top fifty metabolic pathways significantly altered between normal and IPF fibroblast cells (Figure S1A). We further assessed this data through pathway enrichment analysis and found that a number of metabolites were mainly involved in amino acid-metabolic pathways (Figure S1B), suggesting the crucial role of amino acid metabolism in IPF. Of these amino acid-metabolic pathways, arginine biosynthesis has recently gained attention, given that targeting arginine reprogramming has emerged as a novel therapeutic strategy in certain auxotrophic cancers.[29] In particular, a rate-limiting metabolic enzyme, ASS1, is crucial for the *de novo* arginine biosynthesis pathway and plays a critical role in maintaining arginine levels in cells. To investigate the role of ASS1 in PF, we evaluated ASS1 expression by immunohistochemical (IHC) analysis in normal lung tissues ($n = 30$) and lung sections from 30 patients with ILDs. Patient samples were further grouped into low and high ASS1 categories, and their clinical characteristics were summarized in Tables S1 and S2. No significant difference of pulmonary function was observed in ILD patients with a low or high level of ASS1 expression (Figures S1C and S1D).

Compared to normal lung tissues, low ASS1 was detected in 73% ($n = 22/30$) of ILD specimens ($p < 0.0001$; Figure S2A). Likewise, a decline of ASS1 signal was found in the tissue sections from IPF patients, whereas more intense ASS1 staining was observed in normal lung tissues (Figure 1A). We noticed that most fibroblastic foci did not display much immunostaining. Strikingly, low levels of ASS1 protein were seen in IPF versus normal tissues at 79% ($n = 11/14$) versus 20% ($n = 6/30$), respectively, and there was an inverse correlation between ASS1 and IPF status ($p = 0.00033$; Figure 1B). To ascertain the expression level of ASS1 protein in fibroblastic foci characterized by accumulation of the α-smooth muscle actin (SMA)-expressing cells, the

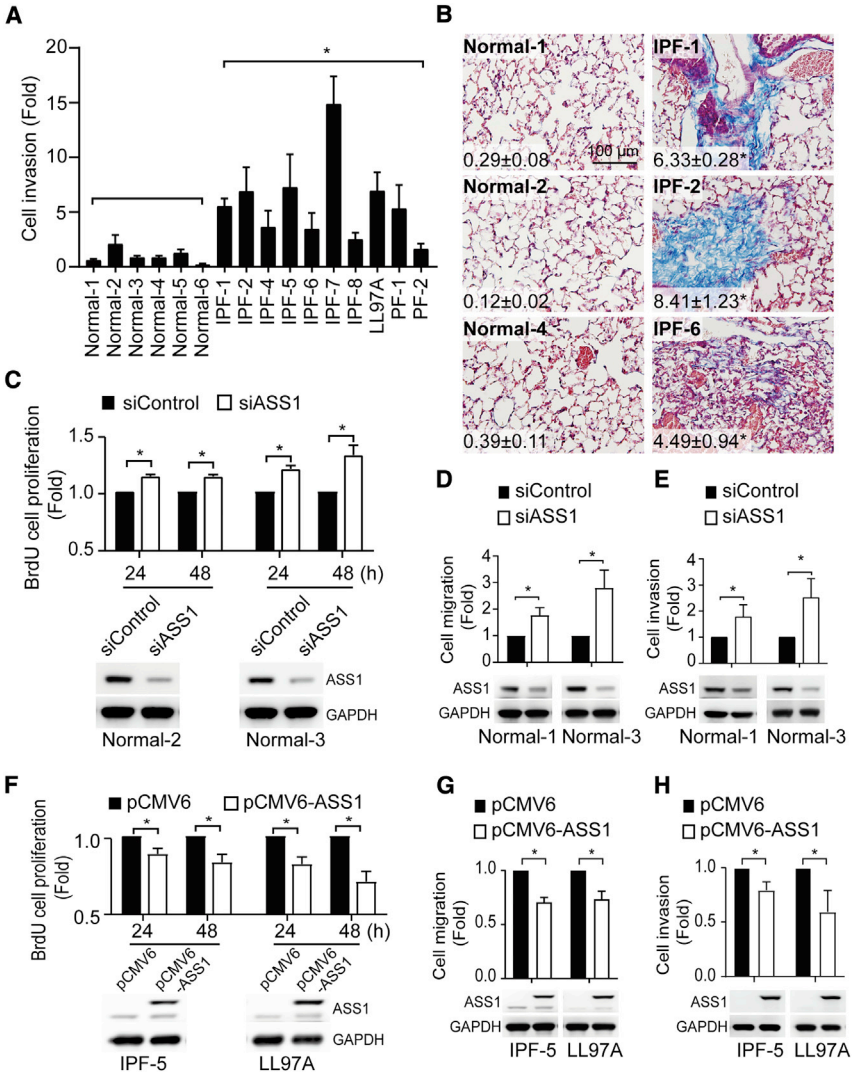

Figure 2. Functional roles of ASS1 in fibrotic lung fibroblasts

(A) The invasion ability of human primary normal fibroblasts and primary IPF fibroblasts, as determined using Matrigel invasion assay. The numbers of invaded cells were counted, and the quantified values of relative invasion ability were normalized to normal-4. *p < 0.05 versus normal (mean ± SE). (B) The lung fibrosis model by an intrapulmonary implantation of primary normal lung fibroblast cells or primary IPF lung fibroblasts. Collagen assessment by Masson's trichrome staining of lungs in tissue specimens from normal or IPF fibroblast-inoculated lungs. Numbers, the fibrosis scores from semiquantitative analysis in Masson's trichrome-stained sections of mouse lung. Fibrosis score is displayed as the percentage of the positive-staining area per high-powered field. 6–12 high-powered fields per lung were analyzed and quantified with ImageJ software. *p < 0.05 versus normal-1. (C) Control siRNAs (siControl)- or ASS1-specific siRNAs (siASS1)-transfected normal fibroblast cells (normal-2 and -3) were subjected to BrdU cell proliferation assays. The cell proliferation rate was determined at 24 h and 48 h. Data are represented as mean ± SE. *p < 0.05. (D and E) Transwell migration and invasion assays of normal fibroblast cells (normal-1 and -3) transfected with control siRNAs or ASS1-specific siRNAs. The cell migration and invasion ability of ASS1-knockdown cells were normalized to that of cells transfected with control siRNAs. *p < 0.05 versus siControl (mean ± SE). (F) BrdU cell proliferation assays of IPF lung fibroblasts (IPF-5 and LL97A) transfected with pCMV6 or pCMV6-ASS1. The cell proliferation rate was examined at 24 h and 48 h. Data are represented as mean ± SE. *p < 0.05. (G and H) pCMV6- or pCMV6-ASS1-transfected IPF lung fibroblasts (IPF-5 and LL97A) were subjected to Transwell migration and invasion assays. The cell migration and invasion ability were quantified and normalized to that of mock transfectants. Data are expressed as mean ± SE. *p < 0.05.

myofibroblasts, human normal, and IPF lung tissue sections were subjected to immunofluorescent staining by using anti-ASS1 and anti-α-SMA antibodies (Figure 1C). We observed weak ASS1 expression in α-SMA-positive fibrotic foci of lung tissues from IPF patients, whereas ASS1 signals were significantly stronger in normal lung tissues, suggesting that ASS1 downregulation is of importance in patients with IPF.

To confirm the dysregulation of ASS1 in IPF fibroblasts, we next assessed the mRNA and protein levels of ASS1 in the above primary lung fibroblast cells derived from healthy donors and IPF patients. As expected, we found that both ASS1 mRNA and protein expression were significantly reduced in IPF lung fibroblasts as compared to all tested primary normal fibroblasts (Figures 1D and 1E). Surprisingly, 3 out of 7 IPF cases showed ASS1 protein deficiency. In a bleomycin (BLM) mouse model of lung fibrosis, IHC data had shown a decrease of ASS1 expression in BLM-exposed lung tissues as compared to those of saline-exposed mice (Figure 1F). Data from immunofluorescent staining further confirmed lower ASS1 signal abundance in α-SMA-expressing fibrotic lung tissues exposed to BLM (Figure 1G). These data suggest that low ASS1 expression is a feature of fibrotic fibroblasts and may play a role in the pathogenesis of PF.

ASS1 expression controls aggressive phenotypes in lung fibroblasts

Since severe fibrosis is propagated by activated fibroblast phenotypes, such as cell invasion and migration,[30,31] we first compared the invasive capabilities of multiple primary human normal and IPF lung fibroblast cells. Data from Transwell invasion assays show an increase in cell invasiveness in all tested primary IPF fibroblasts correlated with low expression of ASS1 and higher levels of α-SMA, a myofibroblast marker (Figures 2A, S2B, and S2C).

Consistently, IPF fibroblasts displayed an elevated migratory ability compared to normal fibroblasts (Figure S2D). To determine that ASS1-deficient IPF fibroblasts exhibit aggressiveness and unfavorable evolution in lung fibrosis, we carried out a lung fibrosis model, modified from an established murine model of PF,[32] by adoptive transfer of primary human pulmonary fibroblasts into severe combined immunodeficiency mice. Fibroblast cells were orthotopically inoculated into the left lobe of mice lung, as we previously reported,[33,34] and we collected the lungs for histological analysis 60 days after inoculation. The lung architecture of mice implanted with normal fibroblasts appeared normal, whereas mice bearing IPF fibroblasts showed disrupted architecture and extensive structural changes in the lungs, concomitant with fibroblastic lesions and deposited ECM (Figure 2B), implying that IPF fibroblasts lacking ASS1 expression were active in persisting, proliferating, and continued collagen deposition compared to normal fibroblasts.

Next, we used ASS1-specific small interfering RNAs (siRNAs) to knock down ASS1 expression in high ASS1-expressing fibroblasts (normal-1, -2, and -3). As shown in Figures 2C–2E, S3A, and S3B, silencing ASS1 expression in primary normal fibroblasts resulted in an increase in fibroblast cell proliferation, migration, and invasion, the crucial cell activities in fibrosis progression. Conversely, a pCMV6-ASS1 construct was introduced into ASS1-deficient IPF fibroblasts (IPF-5 and LL97A; Figures 1E and S3C). After 48 h of transfection, we observed a significant decrease of cell proliferation, migration, and invasion ability in IPF fibroblasts with ectopic expression of ASS1, as compared to the mock controls (Figures 2F–2H and S3D). Altogether, our results provide evidence that aggressiveness of IPF lung fibroblast and fibrosis progression is attributed to ASS1 deficiency.

Loss of ASS1 expression activates Met receptor and its downstream signaling

To further profile signaling networks regulated by ASS1, both control and ASS1-knockdown cells were subjected to reverse-phase protein arrays (RPPAs), followed by the analysis with the Database for Annotation, Visualization and Integrated Discovery (DAVID) pathway analysis tool (https://david.ncifcrf.gov). These pathway analyses identified several RTK-mediated signaling pathways in the top twenty pathways that were significantly affected by ASS1 (Figure 3A). Figure 3B shows a heatmap of the top differentially expressed proteins involved in these RTK pathways. Given the importance of RTKs in fibroblast activities and fibrotic progression,[15] we therefore performed a phospho-RTK array screen and identified four top-ranked RTKs with upregulated tyrosine phosphorylation in both ASS1-deficient IPF (IPF-4) lung fibroblast cells and ASS1-knockdown normal (normal-3) fibroblast cells (Figure 3C, left). Figure 3C (right) lists the four top-ranked RTKs with respect to tyrosine phosphorylation upregulation in response to ASS1 loss. Of these RTKs, the Met receptor (HGFR) was the first to draw our attention, given recent reports showing the implications of Met activation in IPF.[16,17]

To validate the regulation of the Met receptor and its downstream signaling by ASS1 expression, cell lysates from control and ASS1-knockdown normal fibroblasts were subjected to immunoblotting. An elevation of Met phosphorylation at Tyr1349, the multifunctional docking site, was observed in normal fibroblast cells with a lack of ASS1 (Figure 3D). The quantified protein expression levels of phospho-Met and its downstream signal proteins, phospho-Src and phospho-STAT3, have confirmed an activation of the Met signaling pathway in ASS1-deficient cells (Figure S4A). These ASS1-knockdown cells also exhibited an increased expression of the myofibroblast marker α-SMA, despite no evident difference in anti-apoptotic effect, as compared to control siRNA-transfected cells (Figure S4B). On the contrary, overexpression of ASS1 in IPF fibroblasts, IPF-5 and LL97A cells, demonstrated downregulation of phospho-Met (Y1349), phospho-STAT3 (Y705), and α-SMA (Figure S4C). With the use of IHC staining, we verified that high phospho-Met (Y1349) levels were detected in fibrotic lung tissues from both IPF patients and BLM-exposed mice (Figure 3E). These observations support the notion that ASS1 expression modulates Met activity and its downstream signaling pathway.

ASS1-deficient lung fibroblasts are vulnerable to arginine deprivation

Due to an inability to synthesize arginine, cells lacking ASS1 expression require the uptake of extracellular arginine for survival, becoming arginine auxotrophs.[25–27] This characteristic has been found in several cancers, and ASS-deficient tumors exhibit sensitivity to arginine deprivation.[26,35,36] Through degrading arginine to citrulline, treatment with arginine deiminase (ADI) or pegylated ADI (ADI-PEG20) was shown to decrease cell proliferation and induce apoptosis in ASS1-deficient tumor cells.[37,38] Given loss and/or downregulation of ASS1 noted in IPF lung fibroblasts (Figure 1), we assumed that ASS1 deficiency results in an intrinsic dependence on extracellular arginine in IPF lung fibroblasts. To determine that arginine starvation approaches, such as arginine-free conditions and ADI treatment, inhibit ASS1-deficient lung fibroblast growth, we investigated the arginine auxotrophic response in both normal and IPF fibroblasts by culturing fibroblast cells in media with 147.5 mg/L L-arginine or without arginine. 3 days after culturing, the proliferation rate of the above cells was measured every 24 and 48 h. Data from 3-(4,5-dimethylthiazol-2-yl)-5-(3-carboxymethoxyphenyl)-2-(4-sulfophenyl)-2H-tetrazolium (MTS) assays show no significant change on cell proliferation at 24 h and 48 h in normal fibroblast cells between arginine-containing and arginine-free medium groups (Figure 4A, top). Remarkably, cell proliferation of all tested IPF fibroblast cells was decreased in arginine-free medium at 24 h and significantly diminished in response to arginine withdrawal at 48 h (Figure 4A, bottom).

We next utilized ADI, an arginine-degrading enzyme, to directly block the uptake of extracellular arginine into cells.[39] A time course study confirmed the stability of ADI in serum containing media ($T_{1/2}$ from 6 to 24 h; Figure S4D). Normal and IPF fibroblasts were treated with various doses of ADI from

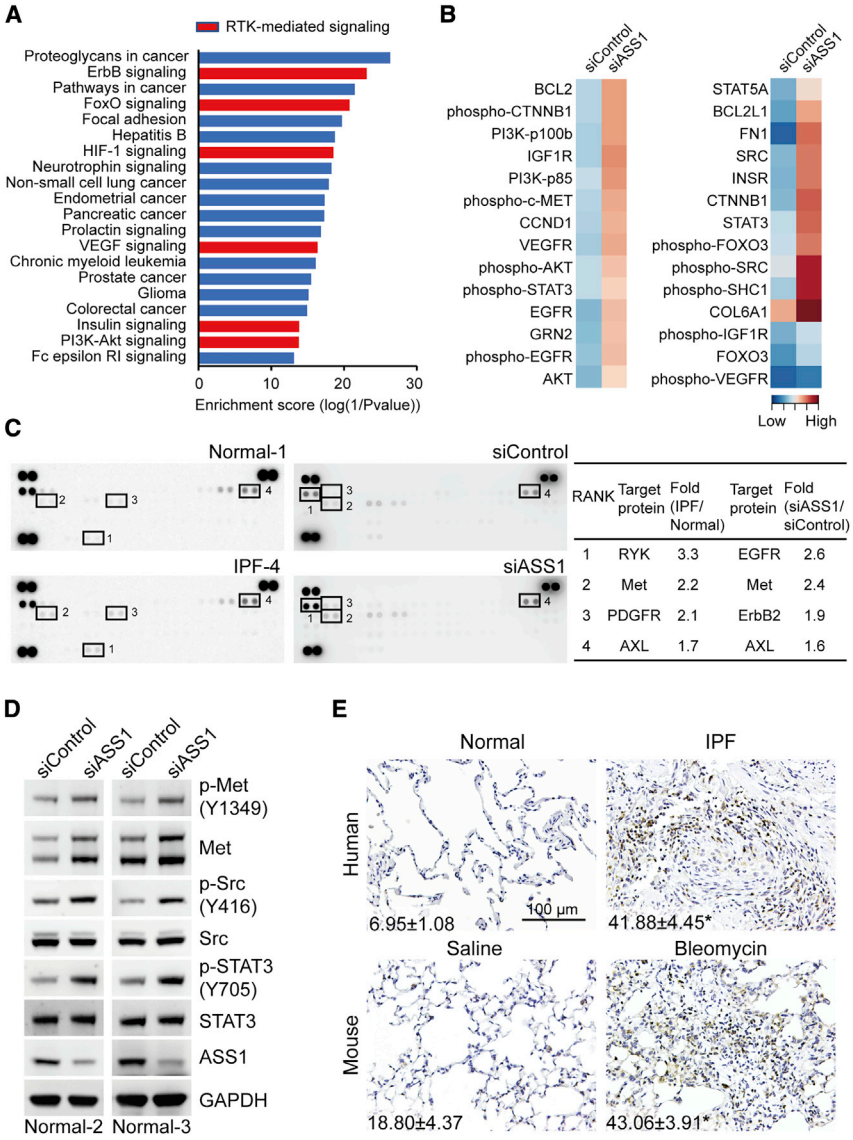

RANK	Target protein	Fold (IPF/ Normal)	Target protein	Fold (siASS1/ siControl)
1	RYK	3.3	EGFR	2.6
2	Met	2.2	Met	2.4
3	PDGFR	2.1	ErbB2	1.9
4	AXL	1.7	AXL	1.6

Figure 3. Activation of Met receptor and its downstream signaling in response to ASS1 loss

(A) DAVID pathway enrichment analysis of the reverse-phase protein array (RPPA) profiles revealed significantly enriched signaling pathways in ASS1-knockdown normal fibroblast cells. The horizontal axis describes the log(1/p value) of the significant pathways. The vertical axis represents the protein clusters involved in the DAVID pathways. (B) Heatmap analysis from RPPA data showing the relative level of total and phosphorylated proteins in normal fibroblast cells with ASS1 knockdown as compared to cells transfected with control siRNAs. Red shades indicate higher intensity, and blue shades represent lower intensity. Data are significant changes as determined by a *p* value threshold of less than 0.05. (C) Left: lysates from primary normal (normal-1) and IPF fibroblasts (IPF-4), as well as siControl-transfected and siASS1-transfected normal fibroblast cells (normal-3) were subjected to human phospho-receptor tyrosine kinase (RTK) array assays. Right: the top four phospho-RTKs in IPF lung fibroblasts and ASS1-knockdown cells are listed. (IPF-4 versus normal-1 and ASS1 siRNA versus control siRNA). (D) Immunoblotting analysis of phospho-Met (Y1349) levels and its downstream molecules Src and STAT3 in two ASS1-knockout normal fibroblast cells (normal-2 and -3). (E) Representative images of immunohistochemical staining using anti-phospho-Met (Y1349) antibody in normal lung tissue and IPF specimens from patients (n = 3,) as well as lung tissues from saline- and BLM-exposed mice (n = 3). Numbers, the percentage of phospho-Met (Y1349)-positive fibroblast cells was quantified by ImageJ software. Data are expressed as mean ± SE. *p < 0.05.

0.25 μg/mL to 2 μg/mL for 72 h and subjected to 3-(4,5-dimethylthiazol-2-yl)-2,5-diphenyltetrazolium bromide (MTT) assays. Figure 4B demonstrates that treatment with ADI significantly impaired cell viability in two tested IPF fibroblasts, and this impairment appeared to be concentration dependent and was more effective in IPF fibroblasts versus normal fibroblast cells. Additionally, lung fibroblasts isolated from saline- or BLM-challenged mice, as described previously,[28] were incubated with increasing concentrations of ADI for 72 h. Cell viability assays confirmed that ADI treatment is very effective in BLM-exposed fibroblasts (Figure 4C). These data suggest that arginine deprivation selectively eradicates arginine-auxotrophic IPF lung fibroblasts without adversely affecting normal fibroblasts.

Arginine deprivation attenuates BLM-induced lung fibrosis in mice

To translate our findings from *in vitro* into *in vivo*, we carried out a BLM-induced PF mouse model.[28] After an intratracheal instillation of BLM, mice were then administered with either an arginine-free diet or ADI intraperitoneally. Figure 5A (top) illustrates the experimental procedure and timelines for arginine deprivation in this study. ADI was intraperitoneally injected into mice during the "fibrotic" phase of the model, which is more applicable and reflective to the clinical management of IPF patients. There were five experimental groups in total: (1) saline plus arginine-containing diet; (2) saline plus arginine-free diet; (3) BLM plus arginine-containing diet; (4) BLM plus arginine-free diet; and (5) BLM plus ADI (225 μg/mL). As shown in Figure 5A (bottom), histological analysis of lung sections from different groups confirmed extensive structural changes in BLM-exposed lungs, whereas decreased fibroblastic lesions were seen in the lungs from these BLM-challenged mice with an arginine-free diet and ADI treatment (Figure 5B). Moreover, BLM-induced upregulation of hydroxyproline levels were

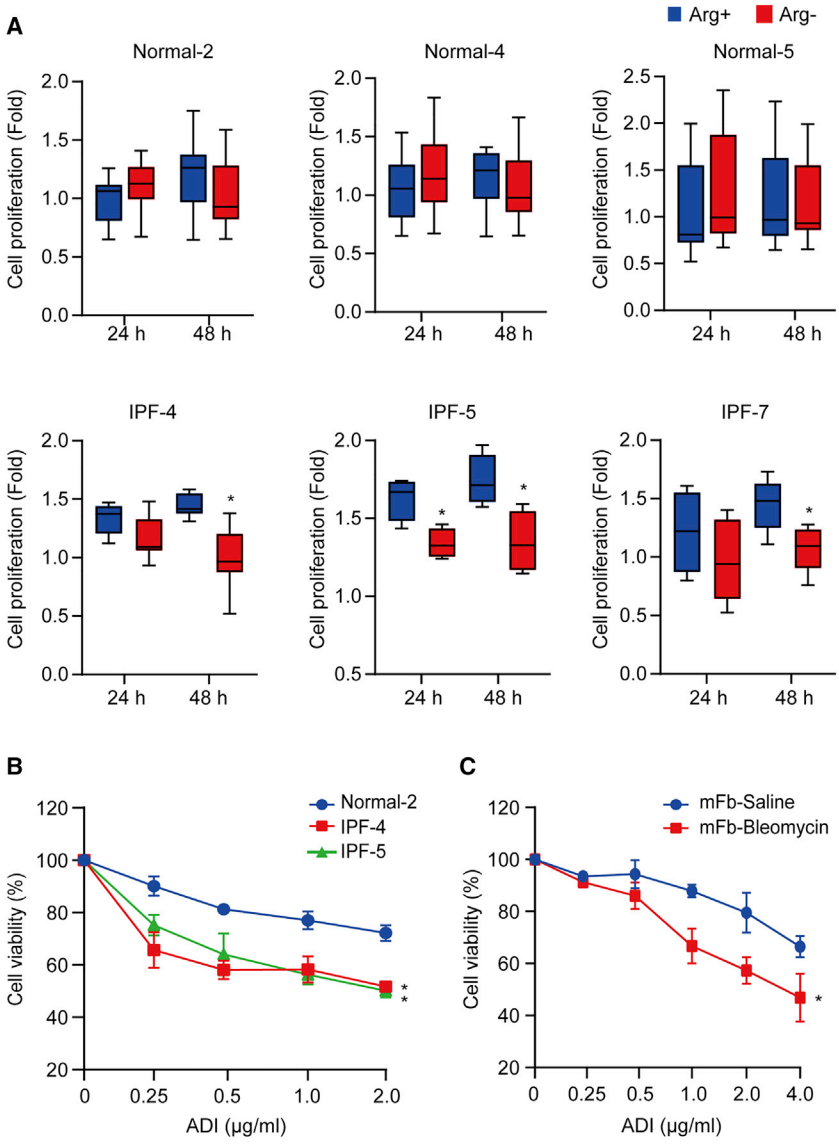

Figure 4. Susceptibility of fibrotic lung fibroblasts to arginine deprivation

(A) Normal (normal-2, -4, and -5) and IPF (IPF-4, -5, and -7) fibroblast cells were incubated in arginine-containing and arginine-free medium for 5 days. After 3 days of incubation, cell proliferation was measured by MTS assay at 0 h (day 3), 24 h (day 4), and 48 h (day 5) and shown as a value relative to 0 h (day 3). Data are represented as mean ± SE from three independent experiments. (*$p < 0.05$ versus arginine-containing medium). (B) Normal (normal-2) and IPF (IPF-4 and -5) fibroblast cells were treated with 0, 0.25, 0.5, 1, and 2 μg/mL of arginine deiminase (ADI) for 48 h (IPF-4) or 72 h (IPF-5). Cell viability was determined by MTT assay. Data are derived from three independent experiments and expressed as mean ± SE. *$p < 0.05$. (C) Effect of ADI on cell viability of lung fibroblasts isolated from saline (mFb-saline)- or BLM (mFb-BLM)-treated mice analyzed using MTT assays ($n = 3$; *$p < 0.05$).

significantly suppressed in both BLM plus an arginine-free diet and BLM plus ADI groups (Figure 5C).

We also evaluated the effect of arginine deprivation on airway inflammation by analysis of the bronchoalveolar lavage fluid (BALF) cell profile (Figure S5). Although there was no obvious difference in immune cell infiltration into lungs among the groups, a slight decrease in the number of macrophages and neutrophils was found in the BALF from both arginine-free diet-treated and ADI-treated mice, indicating a trivial influence of arginine deprivation on regulating the lung inflammatory response. We then determined the effect of arginine deprivation on immune cell profiling in both BALF and the spleen, the largest organ of the lymphatic system. After wild-type C57BL/6J mice were fed with an arginine-containing diet or arginine-free diet for 15 days, immune cells were isolated and subjected to flow cytometry analysis. The data revealed no distinct changes in the percentage of macrophages, neutrophils, and T cells from BALF between arginine-containing and arginine-free diet groups (Figure S7A). Similarly, no significant changes in the immune cell populations, including macrophages, total T, $CD4^+$ T, $CD8^+$ T, natural killer (NK), NKT, and B cells, were found in response to arginine deprivation (Figure S7B). We further incubated Jurkat (T cell line) and ST486 (B cell line) cells, as well as primary mouse BAL cells, with arginine-containing or arginine-free medium for 72 h. Both *in vitro* cell lines and *ex vivo* BAL studies demonstrated no notable effect of arginine starvation on cell viability of all tested immune cells (Figures S7C–S7E).

In an attempt to compare the antifibrotic effects between ADI (225 μg/mL/mouse) and nintedanib (28 mg/kg/mouse), we conducted the other cohort of BLM-induced PF studies. Surprisingly, only ADI-treated mice exhibited a higher percentage survival after BLM challenge, whereas nintedanib-treated mice did not ($p = 0.08$, log-rank test; Figure 5D). These results suggest a promising therapeutic application of arginine-deprivation approaches in treating PF.

Arginine deprivation increases nintedanib efficacy

Since loss of ASS1 in lung fibroblasts activated the Met receptor (Figure S8A), which is not a target of nintedanib, ASS1-deffcient IPF fibroblasts may continue growth via Met signaling during nintedanib treatment. Indeed, most IPF fibroblasts exhibited unresponsiveness to nintedanib with the IC_{50} (half-maximal inhibitory concentration) higher than 10 μM (Figure S8B). Given an arginine auxotrophic response in IPF lung fibroblasts, we proposed that nintedanib combined with arginine-deprivation conditions enhances its efficacy

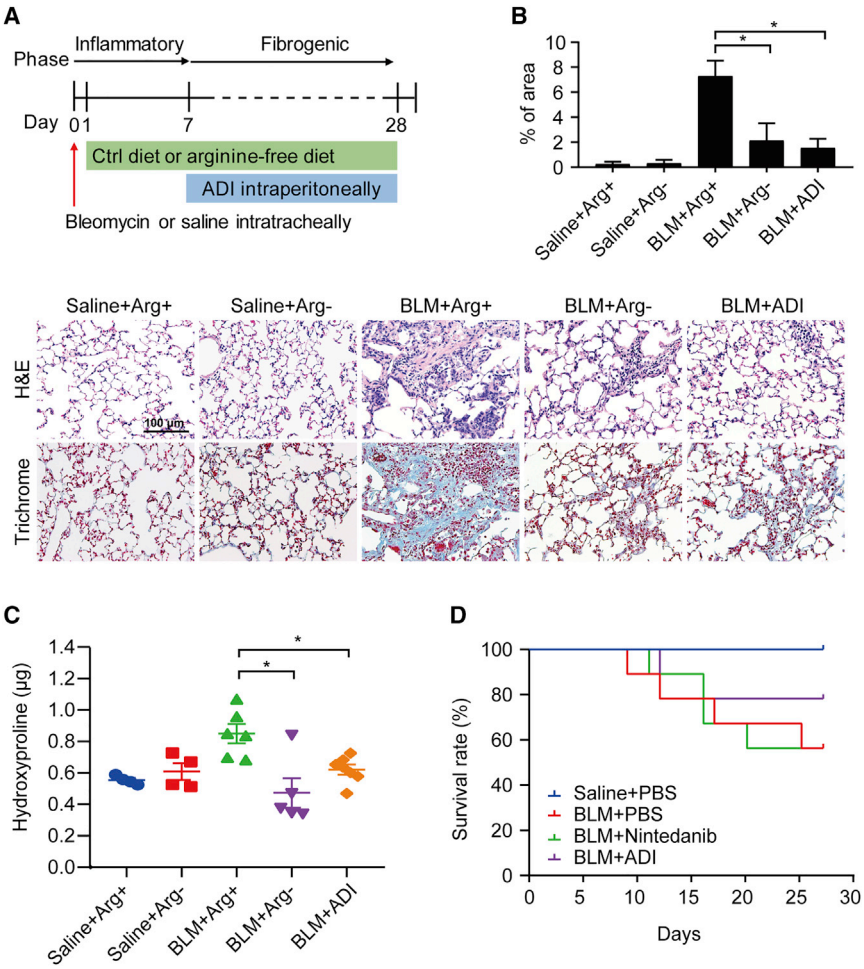

Figure 5. The therapeutic potential of arginine deprivation in halting lung fibrosis

(A) Top: experimental timeline in BLM-induced pulmonary fibrosis with or without arginine diet and ADI treatment (n = 8 mice/group). After C57BL/6J mice intratracheally received saline or BLM (0.005 U/g), the mouse diet was replaced with isonitrogenous control diet or arginine-free diet on the next day. At day 7, the BLM-exposed mice were intraperitoneally given ADI at a dosage of 225 μg/mL every day. At day 28, mice were euthanized, followed by lung harvest. Bottom: representative photomicrographs of hematoxylin and eosin (H&E)- and Masson's trichrome-stained lung sections with various treatments. (B) Semi-quantitative histopathological scoring of positive staining on Masson's trichrome-stained sections of mouse lung. Fibrosis score is determined as the percentage of the positive staining area per high-powered field. Quantification of 6–12 high-powered fields per lung was performed with ImageJ software. *$p < 0.05$. (C) Hydroxyproline levels in the right lung of mice were determined by the hydroxyproline ELISA assay. Data are expressed as mean ± SE (*$p < 0.05$ versus BLM + arginine-containing diet). (D) Saline- and BLM-exposed mice were grouped into PBS, nintedanib, or ADI treatment, and their overall survival rates of mice were analyzed by a Kaplan-Meier survival plot (n = 8 mice/group).

through inhibition of Met-mediated cell survival signaling (Figure S8C). To this end, IPF lung fibroblasts were treated with nintedanib in media with or without arginine for 72 h. As we expected, cell viability was significantly decreased in nintedanib-treated lung fibroblasts incubated with arginine-free medium as compared to those with arginine-containing medium (Figure 6A). In addition, IPF fibroblasts were treated with various doses of nintedanib (0.625–4 μM) and/or ADI (0.625–4 μg/mL) for 72 h. Cotreatment of nintedanib with ADI showed superior viability inhibition as compared to nintedanib monotherapy (Figure S8D). To evaluate the therapeutic interactions between nintedanib and ADI, we used the Chou and Talalay[40] CI (combination index) method and demonstrated that the CI values for the two drugs were lower than 1 in both IPF-4 and IPF-5 cells (Figure 6B), implying the synergistic effect of drug combination. Simultaneously, cell survival was significantly lower with the combination treatment (Figure 6C).

We further examined the synergistic effect of nintedanib and arginine deprivation in a mouse model of BLM-induced PF, and the timeline of this experimental procedure for combined treatment was illustrated in Figure 6D. Nintedanib and/or ADI were intraperitoneally injected into BLM-exposed mice during the fibrotic phase (day 7) of the model. There were four therapeutic regimens in BLM-exposed mice, including the following: (1) PBS only, (2) 14 mg/kg nintedanib only, (3) 112.5 μg/mL ADI only, and (4) 14 mg/kg nintedanib combined with 112.5 μg/mL ADI. Histological analysis of lung sections demonstrated marked fibrotic lesions in BLM-exposed mice receiving PBS or monotherapy only, whereas BLM-induced fibroblastic lesions were markedly reduced in mice treated with nintedanib combined with ADI therapy (Figure 6E). Consistent with histological analysis, BLM-challenged mice with combination therapy displayed lower levels of hydroxyproline in the lungs (Figure 6F). Analysis of BALF cell profiling confirmed a slight effect of nintedanib combined with ADI on modulation of airway inflammatory response (Figure S9). These data convincingly demonstrate that arginine deprivation enhances nintedanib efficacy in IPF lung fibroblasts.

DISCUSSION

The role of dysregulated metabolism in IPF has only been appreciated in recent years.[19–22,41] In agreement with prior studies showing that upregulation of arginine metabolism and metabolites (e.g., polyamine, creatine, and 4-hydroxyproline) in this pathway was noted in IPF lung tissues,[21,22] our current metabolomics data have demonstrated a dysregulated arginine metabolism in IPF lung fibroblasts and pointed out the implications of this metabolic pathway in lung

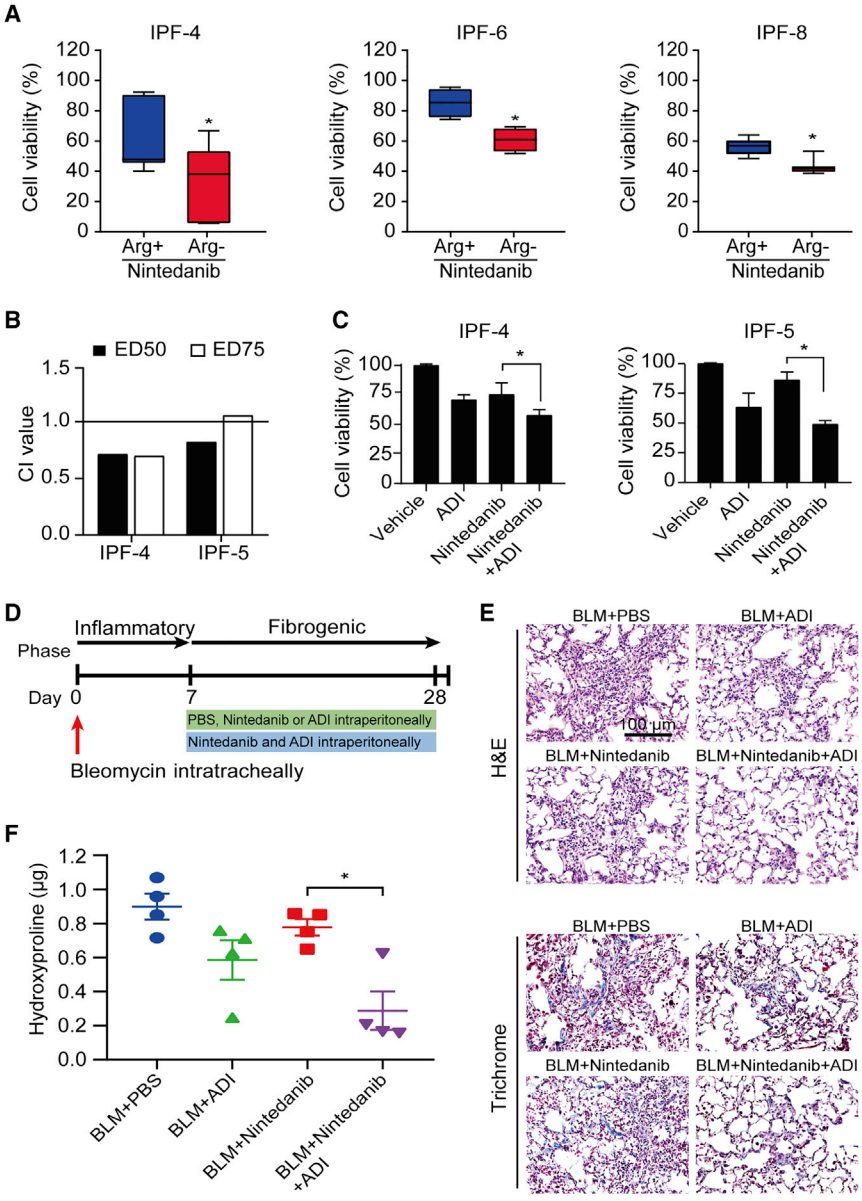

Figure 6. The effect of arginine deprivation in increasing nintedanib efficacy

(A) IPF (IPF-4, -6, and -8) fibroblast cells were treated with 10 μM of nintedanib in arginine-containing and arginine-free medium for 72 h. Cell viability was assessed by MTT assays. Data are expressed from three independent experiments (*$p < 0.05$ versus arginine-containing medium + nintedanib). (B) The combination index (CI) method was utilized to analyze the therapeutic effects of drug interactions between nintedanib and ADI using the CalcuSyn software. CI defines synergism (CI < 1), additive effect (CI = 1), and antagonism (CI > 1). Additive effect of the combination treatment is indicated by a black line at CI = 1. (C) IPF fibroblasts were treated with 4 μM of nintedanib alone, 4 μg/mL of ADI, or combinations of nintedanib at 4 μM and ADI at 4 μg/mL for 72 h. The cell viability was measured by MTT assays. Data are derived from three independent experiments and expressed as mean ± SE (*$p < 0.05$ compared with nintedanib). (D) Experimental timeline for BLM-induced pulmonary fibrosis in mice treated with PBS, nintedanib, ADI, or nintedanib plus ADI ($n = 4$ mice/group). C57BL/6J mice intratracheally received BLM (0.005 U/g). At day 7, the BLM-exposed mice were intraperitoneally given PBS (BLM + PBS), ADI only (BLM + ADI), nintedanib only (BLM + nintedanib), and nintedanib plus ADI (BLM + nintedanib + ADI). At day 28, mice were euthanized followed by collection of lungs for further analysis. (E) Representative photomicrographs of H&E-stained and Masson's trichrome-stained lung sections with various treatments. (F) Levels of hydroxyproline in the right lungs of mice were measured by a hydroxyproline ELISA assay. Data are expressed as mean ± SE.

fibrogenesis. In this study, we have identified and characterized the functional role of ASS1 as the component of the arginine metabolic pathway contributing to the RTK signal transduction and profibrotic phenotypes in lung fibroblasts. In addition, we present a proof of concept for the use of ADI or an arginine-free diet to selectively eradicate fibrotic fibroblasts without adversely affecting normal fibroblasts, leading to mitigating fibrosis progression.

As arginine metabolism is dysregulated in IPF,[21] critical components of this pathway, such as ASS1, the rate-limiting enzyme in the biosynthesis of arginine, are likely altered. We have identified a marked downregulation of ASS1 in both tissues and cells isolated from IPF patients as well as in the BLM model of PF. This decrease in expression is closely associated with PF status, particularly with IPF, with IPF patient tissues making up roughly 50% of the ILD tissues in our cohort. Additionally, we show that ASS1 deficiency promoted invasive and fibrotic potential in lung fibroblasts. Although biomarkers for IPF do exist, there is still a lack of reliable markers for IPF, and very few metabolic enzymes have been shown to be associated with IPF status.[42] In conjunction with other markers, ASS1 could serve to distinguish IPF from other lung malignancies. These observations taken together suggest that ASS1 is an excellent candidate biomarker.

Beyond its potential as a discriminating factor for fibrotic tissue and aberrant fibroblasts, ASS1 also plays a functional role in lung fibroblasts. We have observed an aggressive phenotype with increased invasiveness, motility, proliferation, and matrix deposition capabilities in ASS1-deficient fibroblasts. Modulation of ASS1 expression can control these phenotypic traits and regulate the progression and development of PF in our animal model. Studies in cancer

have demonstrated ASS1 acts as a tumor suppressor.[43,44] Our findings indicate that ASS1 operates in a similar fashion in lung fibroblasts; high levels of ASS1 have a notable suppressive effect on proliferation and invasion, whereas low levels have an opposite effect. To our best knowledge, this is the first report of a ASS1 contribution in controlling fibroblast behaviors.

Given the functional role of ASS1 deficiency, we next investigated the potential mechanisms through which ASS1 controls fibroblast cell behavior. RTKs have recently been demonstrated as major drivers of fibrotic progression with roles in lung fibroblasts.[15] In our functional proteomic analysis of ASS1-manipulated cells, we had observed many RTK-associated signaling pathways upregulated in response to ASS1 knockdown, suggesting that there was an interplay between the metabolism with signal transduction pathways. Further analysis of the RTKs involved identified Met as a top candidate RTK downstream of ASS1. Met is a well-studied oncogenic receptor playing roles in cell proliferation and invasive phenotypes.[13,18,45] In ASS1-deficient fibroblasts, we found that Met can mediate downstream Src and STAT3 signaling activity, driving an aggressive and anti-apoptotic phenotype. Although prior studies have already implicated Met in PF,[16,17] the trigger for its activation remains unclear. Herein, we have identified ASS1 as a regulator of Met activity and demonstrate a novel signal circuit: the ASS1-Met-Src-STAT3 signaling axis. There may be multiple mechanisms through which ASS1 acts on Met, and the exact mechanism of regulation is an area of further study.

The targeting of aggressive fibroblasts, the key players in IPF development and progression, has long been an enticing approach.[46] However, approaches targeting these cells thus far have been marred by specificity issues and adverse effects.[46,47] We, corroborated with other groups, have identified Met as a key molecule in IPF fibroblasts,[16,17] suggesting that it is an obvious target choice. However, Met inhibitors have had similar disadvantages as other drugs in their class.[48] Nonspecific inhibition of other receptors and targeting of other cell types have been key issues preventing specific ablation of aggressive fibroblasts. Other antifibrotics, to date, and in particular pirfenidone and nintedanib, affect a spectrum of cells and can modulate inflammation[5,49] and are not specific therapeutics targeting lung fibroblasts.

How then can we specifically target aberrant fibroblasts in IPF? ASS1 is a crucial enzyme in arginine synthesis;[24] without ASS1, cells cannot synthesize their own arginine and are reliant on import of extracellular arginine.[25–27,35,36,38] Normal cells have endogenous levels of ASS1 and can synthesize arginine, whereas IPF cells have a reduced or no capability to do so. Taking advantage of this phenomenon, we could specifically target IPF fibroblasts through blockading extracellular sources of arginine. As a proof of concept, we utilized arginine-deficient media/diet and enzymatic degradation of arginine with ADI approaches. Both approaches were effective at selectively inhibiting IPF cells, while leaving normal cells relatively unharmed, indicating our proposed strategy functioned as intended. These findings were further reflected in the BLM mouse model of PF, where arginine depletion strategies were able to reduce overall histologic fibrosis and ECM deposition. Of note, this effect was not mediated through alteration of airway inflammation, suggesting that arginine depletion directly acts upon lung fibroblasts. These approaches offer a novel and direct way to target activated fibroblasts in IPF.

A previous study by Harm Maarsingh et al.[50] demonstrated that increased arginase activity is likely associated with fibrotic disorders of the lung. Higher arginase activity may promote conversion of L-arginine into L-ornithine and urea and lead to arginine deficits in the cells. This observation is consistent with what we found in our studies. Downregulated ASS1 in IPF fibroblasts results in the inability of the cells to catalyze the biosynthesis of arginine (arginine auxotrophy) and leads to insufficient amounts of arginine in those fibroblasts. Hence, we assessed the utility of arginine deprivation in halting disease progression in the fibrogenic phase of BLM-challenged mice. Prior work by Gao et al.[51] seems contrary to our study and seems to demonstrate that a combination of L-arginine and L-norvaline treatment could inhibit BLM-induced lung fibrosis progression; however, the oral administration of L-arginine was started in an inflammatory phase, not in a fibrogenic phase in that study. This is likely due to the timing of arginine administration; the effect of arginine may play different roles in regulating inflammatory response and fibrotic progression of BLM-induced lung fibrosis in mice, leading to distinct outcomes dependent on when arginine levels are modulated.

Although arginine depletion shows promise as a therapeutic approach, there may be benefit in pursuing combinatorial approaches to improve current drugs and enhance targeting of activated fibroblasts. The current FDA-approved drug nintedanib can suppress multiple pathways involved in lung fibrosis;[5] however, it is unable to target Met signaling. As we show Met activation in IPF cells, Met signaling may be a potential bypass mechanism for aberrant fibroblasts, allowing for continued cell proliferation and invasion. This could offer an explanation as to why nintedanib is limited in therapeutic efficacy;[2,9,10] Met signaling is still active, and IPF fibroblasts can rely on this signaling pathway to support their aggressive phenotypes. Shutting down Met signaling in conjunction with other RTK pathways is a promising approach to effectively target aberrant fibroblasts. We demonstrate that nintedanib, in combination with the specificity of targeting Met signaling through arginine depletion, offers superior and synergistic targeting of IPF fibroblasts. This approach may help address the shortcomings of nintedanib monotherapy and is a potential and viable method to address progressive fibrosis.

To our best knowledge, our study is the first report of the functionality of ASS1 in fibroblast cells and the novel ASS1-Met-Src-STAT3 signaling circuit. With the exploitation of the role of ASS1 in modulating Met activity, we demonstrate that extracellular arginine depletion is a selective and efficacious approach to targeting the aberrant fibroblast and is a promising therapeutic avenue that merits further validation and study. Additionally, the combinatorial approach of arginine depletion and nintedanib is a promising approach and justifies further study. In summary, ASS1 presents itself as a promising

biomarker, and targeting of cells deficient in ASS1 could be a viable and potential therapeutic avenue.

MATERIALS AND METHODS

Reagents and antibodies

Dulbecco's modified Eagle's medium (DMEM), RPMI-1640, fetal bovine serum (FBS), penicillin-streptomycin, Opti-MEM, and red blood cell (RBC) lysis buffer were purchased from Gibco, Thermo Fisher Scientific (Waltham, MA, USA). DMEM/Ham's F-12 medium 1:1 (DMEF), with and without L-arginine, was purchased from Caisson Labs (Smithfield, UT, USA). Vectastain Elite ABC Kit (rabbit immunoglobulin G [IgG]), 3,3′-diaminobenzidine (DAB) solution, and Vector Hematoxylin QS nuclear counterstain were purchased from Vector Laboratories (Burlingame, CA, USA). Anti-phospho-Met (Tyr1349), anti-Met, anti-phospho-Src (Tyr416), anti-Src, anti-phospho-STAT3 (Tyr705), anti-STAT3, anti-poly (ADP-ribose) polymerase (PARP), anti-caspase-3, and anti-glyceraldehyde 3-phosphate dehydrogenase (GAPDH) were purchased from Cell Signaling Technology (Danvers, MA, USA). Anti-phospho-Met (Tyr1349) was purchased from Abcam (Cambridge, MA, USA). α-SMA was purchased from ARP (American Research Products; Waltham, MA, USA). Anti-ASS1 and Lipofectamine 2000 Transfection Reagent were purchased from Invitrogen, Thermo Fisher Scientific (Waltham, MA, USA). Human phospho-RTK Array Kits were purchased from Research and Diagnostic Systems (Minneapolis, MN, USA). ADI was purchased from PeproTech (Cranbury, NJ, USA). Ghost Dye Violet 510, PE-Cy5 CD3ε, Brilliant Violet 570 CD4, PE-Cy7 CD8a, allophycocyanin (APC)-Fire750 CD11b, Brilliant Violet 785 CD19, PE/Dazzle 594 DX5, Alexa Fluor 700 F4/80, Brilliant Violet 650 Ly-6C, and Brilliant Violet 711 Ly-6G were obtained from BioLegend (San Diego, CA, USA). Nylon mesh for flow cytometry assays was purchased from (Becton Dickinson [BD] Falcon, Bedford, MA, USA). Hydroxyproline assay kits were purchased from Millipore Sigma (Burlington, MA, USA).

Cell culture

IPF lung fibroblast cells were established from patients with histologically confirmed IPF who underwent biopsies at the University of California, Davis (UC Davis), Medical Center, as described previously.[28] In all patients, the diagnosis of IPF was verified by the history of disease, lung function tests, microscopic analysis of lung tissue, and the pattern of usual interstitial pneumonia (UIP) on high-resolution computed tomography (HRCT). This investigation was approved by the Institutional Review Board of the UC Davis Health System. Written, informed consent was obtained from all patients. Normal human lung fibroblasts were derived from individual postmortem human airway samples or histologically normal tumor-adjacent lung tissues. The IPF fibroblast cell line LL97A cells, T cell line Jurkat cells, and B cell line ST486 cells were purchased from the American Type Culture Collection (ATCC) (Manassas, VA, USA). All fibroblast cells were maintained in high-glucose DMEM, supplemented with 10% FBS and 1% penicillin-streptomycin at 37°C under a humidified atmosphere with 5% CO_2.

siRNA design, overexpression plasmids, and transfection

ON-TARGETplus ASS1 siRNA and ON-TARGETplus control siRNA were designed and synthesized by Dharmacon, Horizon Discovery (Lafayette, CO, USA). Cells were grown to 50% confluence, and transfection was mediated using the Lipofectamine 2000 Transfection Reagent, according to the manufacturer's instructions (Invitrogen). Briefly, the cells were transfected with 60 nM of ASS1 siRNA or control siRNA in Opti-MEM for 8 h. The cells were then incubated in fresh complete medium for at least 24 h. The Myc-DDK-tagged ASS1 was expressed in mammalian cells by using a pCMV6-Entry construct (OriGene, Rockville, MD, USA). For ectopic expression of Myc-DDK-tagged ASS1 in IPF fibroblast cells, cells were transfected with 3 μg of pCMV6 or pCMV6-ASS1 plasmids using the Lipofectamine 2000 Transfection Reagent, according to the manufacturer's protocols (Invitrogen).

Patient specimens and IHC staining

Normal and IPF lung tissue specimens were obtained from patients who underwent curative surgery or had histologically confirmed IPF at the UC Davis Medical Center. This investigation was approved by the Institutional Review Board of the UC Davis Health System. Written, informed consent was obtained from all patients. All patient samples were de-identified and provided by the UC Davis Interstitial Lung Disease Program. Formalin-fixed and paraffin-embedded specimens were used, and the levels of ASS1 and phospho-Met (Y1349) were analyzed by IHC staining, as described previously.[28,34] Detailed experimental procedures were modified from the paraffin immunohistochemistry protocol supplied by the manufacturer (Cell Signaling Technology, Danvers, MA, USA). The slides were de-paraffinized in xylene substitute and rehydrated in graded alcohol and water. An antigen retrieval step (10 nM sodium citrate [pH 6.0] at a sub-boiling temperature) was used for each sample. Endogenous peroxidase activity was blocked by 3% hydrogen peroxide, followed by blocking serum and incubation with appropriate antibodies overnight at 4°C. Detection of immunostaining was carried out by using the VECTASTAIN ABC system, according to the manufacturer's instructions (Vector Laboratories, Burlingame, CA, USA). A four-point staining intensity scoring system was devised to confirm the relative expression of ASS1 in lung specimens; scores ranged from zero (no expression) to 3 (highest-intensity staining), as described previously.[28,34,52,53] The results were classified into two groups according to the intensity and extent of staining: in the low-expression group, staining was observed in 0%–1% of the cells (staining intensity score = 0), in less than 10% of the cells (staining intensity score = 1), or in 10%–25% of the cells (staining intensity score = 2); in the high-expression group, staining was present in more than 25% of the cells (staining intensity score = 3).

Quantitative real-time PCR

Total RNA was extracted from fibroblast cells using the TRIzol reagent (Invitrogen, Carlsbad, CA, USA). cDNAs were reversely transcribed using SuperScript III Reverse Transcriptase (Invitrogen). The ASS1 and TATA-binding protein (TBP) primers used were as follows: ASS1 forward primer 5′-TGGGCTTGAAATTTGCTGAGCTG-3′

and reverse primer 5′-CGATGCAGTGGCGGACAAATTC-3′; TBP forward primer 5′-CACGAACCACGGCACTGATT-3′ and reverse primer 5′-TTTTCTTGCTGCCAGTCTGGAC-3′. The housekeeping gene TBP was utilized as the reference gene in quantitative real-time RT-PCR assay. Quantitative real-time RT-PCR was conducted using the SYBR Green system and performed according to manufacturer's instructions of the ViiA 7 Real-Time PCR System (Applied Biosystems, Thermo Fisher Scientific, Waltham, MA, USA). The relative expression level of the ASS1 gene compared with that of the TBP was defined as $-\Delta CT = -[CT_{ass1} - CT_{tbp}]$. The ASS1/TBP mRNA ratio was calculated as $2^{-\Delta CT} \times K$, where K is a constant.

Immunofluorescence

The tissue slides were de-paraffinized, rehydrated, and heated for antigen retrieval. After the tissue slides were incubated with primary antibody (anti-ASS1 and anti-α-SMA) overnight at 4°C, the tissue sections were then incubated with Alexa 488-conjugated antibody or Alexa 568-labeled antibody for 1 h at room temperature in the dark. The nuclei were subsequently stained with 4′,6-diamidino-2-phenylindole (DAPI). After the slides were mounted in mounting medium, the detection of immunofluorescence was performed using the FluoView FV3000 spectral confocal system (Olympus, Center Valley, PA, USA).

Immunoblotting

The total cell lysates of fibroblast cells were prepared with lysis buffer (50 mM Tris-HCl [pH 7.4], 1% Triton X-100, 10% glycerol, 150 mM NaCl, 1 mM EDTA, 20 mg/mL leupeptin, 1 mM PMSF, and 20 mg/mL aprotinin). Proteins were separated via SDS-PAGE and transferred to polyvinylidene fluoride (PVDF) membranes. Appropriate antibodies were probed on the membranes, followed by enhanced chemiluminescence detection. The images of immunoblotting analysis were quantified by ImageJ software (National Institutes of Health, Bethesda, MD, USA).

RPPA

More than 1×10^6 control or ASS1 siRNA-transfected normal fibroblast cells were collected and submitted to the RPPA Core Facility, MD Anderson Cancer Center (Houston, TX, USA), for RPPA analysis. Proteins and phosphorylated proteins were selected according to their involvement in crucial cellular functions and signaling pathways.

Human phospho-RTK array

The Human Phospho-RTK Array Kit (#ARY001B) was purchased from R&D Systems (Minneapolis, MN, USA). We performed array screening according to the manufacturer's protocol. Briefly, cell lysates were incubated with the phospho-RTK array membranes. After washing, the membranes were incubated with biotinylated antibody cocktail. The amounts of phospho-RTK were assessed with streptavidin conjugated to horseradish peroxidase, followed by chemiluminescence detection. The density of each dot was quantified and against the average of the internal controls on the membrane, as indicated in the protocol.

Cell proliferation and viability assays

Cells were seeded onto 96-well plates at a density of $5-10 \times 10^3$ cells per well and cultured for the indicated treatment. Cell proliferation was evaluated using an MTS assay kit (Promega, Madison, WI, USA) and bromodeoxyuridine (BrdU) cell proliferation assay kit (Cell Signaling Technology, Danvers, MA, USA). 20 μL of the combined MTS/phenazine methosulfate (PMS) solution was added into each well, incubated for 3 h at 37°C, and the absorbance was measured at 490 nm by using an ELISA reader (Synergy H1; BioTek Instruments [BioTek], Winooski, VT, USA). For the BrdU cell proliferation assay, BrdU incorporation and assays were performed according to the manufacturer's instructions. After 100 μL stop solution was added into each well, the absorbance was measured using an ELISA reader (Synergy H1; BioTek, Winooski, VT, USA) at 450 nm. For an MTT assay, cells were seeded into 96-well plates, grown to 75% confluence, and cultured for the indicated treatment. Cell viability was evaluated by the MTT assay, according to the manufacturer's protocol (Millipore Sigma, Burlington, MA, USA).

Cell-invasion, migration, and scratch wound-healing assays

An *in vitro* cell-invasion assay was performed as previously described[28,33,34] using Transwell chambers (8 μm pore size; Costar, Cambridge, MA, USA). Briefly, 2×10^4 cells were seeded on top of the polycarbonate filters coated with Matrigel (Becton Dickinson, Franklin Lakes, NJ, USA), and 0.5 mL of growth medium was added to both the upper and lower wells. After incubation for 20 h, filters were swabbed with a cotton swab, fixed with methanol, and then stained with Giemsa solution (Millipore Sigma, Burlington, MA, USA). The cells attached to the lower surface of the filter were counted under a light microscope (10× magnification). For the cell migration assay, 1×10^4 cells were seeded on top of the polycarbonate filters with 0.5 mL of growth medium. After incubation for 20 h, the following steps were the same as described for cell-invasion assays. For a wound-healing assay, cells were seeded to six-well tissue-culture dishes and grown to confluence. Each confluent monolayer was then wounded linearly using a pipette tip and washed three times with PBS. Thereafter, cell morphology and migration were observed and photographed at 12 and 24 h. The number of cells migrating into the cell-free zone was acquired under a light microscope.

Patient-derived PF model

The lung fibrosis model by adoptive transfer of human pulmonary fibroblasts to severe combined immunodeficiency mice is modified from an established murine model of PF.[32] 6-week-old C.B-17 SCID/bg mice (supplied by Charles River Laboratories) were housed four mice per cage and fed autoclaved food *ad libitum*. Primary lung fibroblasts (2×10^5 cells in 50 μL PBS containing 10 ng Matrigel) were inoculated into the left lung of mice, as we previously reported.[33,34,54,55] 60 days after injection of fibroblasts, these mice were sacrificed, and the lungs were collected for histological analysis using Masson's Trichrome Staining Kit (Millipore Sigma, Burlington, MA, USA). The present animal study was approved by the Institutional Animal Care and Use Committees (IACUC) at UC Davis.

BLM-induced PF model

The procedures involving mouse experiments were approved by the IACUC of UC Davis. C57BL/6J female mice were purchased from The Jackson Laboratory (Bar Harbor, ME, USA). 4 mice per cage were housed and fed with rodent laboratory chow *ad libitum*. 8-week-old C57BL/6J mice were exposed to saline or BLM by intratracheal instillation, as previously described.[28,56] Briefly, mice were anesthetized with 5% isoflurane and then intratracheally injected with sterile saline or 0.005 U/g BLM (EMD Millipore, Billerica, MA, USA) on day 0. The next day, saline- and BLM-exposed mice were started on a control (arginine-containing) diet (TD.01804) or an arginine-free diet (TD.09152) (Envigo Teklad Diet, Madison, WI, USA). BLM-exposed mice received intraperitoneal administrations daily with ADI (225 μg/mL) from day 7 in the early fibrogenic phase. At the end of BLM insult (day 28), the mice were euthanized, and their lungs were collected for histological (H&E and Masson's trichrome staining) and hydroxyproline content analysis. For nintedanib combined with ADI treatment, BLM-exposed mice received intraperitoneal injections with nintedanib (14 mg/kg) every other day and/or daily with ADI (112.5 μg/mL) from day 7. Intraperitoneal administrations daily with PBS for BLM-exposed mice served as the control group. The mice were euthanized at the end of BLM insult (day 28), and the lungs were harvested for histological and hydroxyproline content analysis.

Collection of BALF

After mice were euthanized at the end of the experiments, an Exel Safelet catheter was inserted into the trachea, securely tied in place with a nylon string. A syringe containing 1 mL PBS was placed in the end of the catheter for gently injecting 1 mL PBS into the lungs. The recovered lavage fluid was transferred into a 15-mL tube and then centrifuged at 500 × *g* for 10 min at 4°C. BAL cells were resuspended in 500 μL RBC lysis buffer and incubated for 30 s. 2.5 mL PBS was subsequently added to stop the reaction, and the lavage fluid was centrifuged at 500 × *g* for 10 min at 4°C. BAL cells were resuspended in 1 mL PBS and then counted. The BAL cells were then subjected to Cytospin for cell staining or utilized for flow cytometry analysis.

Flow cytometry assays

Both BAL and spleens were removed from euthanized animals, and single-cell suspensions of leukocytes were prepared by disaggregation of the tissue through a 100-μm nylon mesh. Cells were washed once with RPMI 1640, supplemented with 10% heat-inactivated FBS (hiFBS), then incubated with RBC lysis buffer for 1 min to remove RBCs, and then washed in RPMI 1640 with hiFBS. Cell isolates were prepared as above, then washed, and resuspended in staining medium (1× PBS, 0.5% BSA, 0.02% sodium azide). Ghost Dye Violet 510 was used for dead cells' staining. Leukocytes were labeled with a combination of the following antibodies: PE-Cy5 CD3ε, Brilliant Violet 570 CD4, PE-Cy7 CD8a, APC-Fire750 CD11b, Brilliant Violet 785 CD19, PE/Dazzle 594 DX5, Alexa Fluor 700 F4/80, Brilliant Violet 650 Ly-6C, and Brilliant Violet 711 Ly-6G. Data were acquired and analyzed using a LSR II flow cytometry and FlowJo software (BD Biosciences).

Hydroxyproline assays

The amount of hydroxyproline was measured in lung tissues using the hydroxyproline assay according to the manufacturer's instructions (Millipore Sigma). Briefly, 10 mg of the right lung was homogenized in 100 μL d.d.H_2O using the sonicator (VC50 Vibra-Cell; Sonics and Materials, Newtown, CT, USA). The lung tissue homogenates were transferred to glass Wheaton ampules (Wheaton, Millville, NJ, USA) and hydrolyzed by adding 100 μL of hydrochloric acid (12 M) for 3 h at 120°C. After samples were centrifuged at 10,000 × *g* for 3 min, the supernatant was collected and transferred to the 96-well plate. The plate was then placed in a 60°C oven to dry samples. 100 μL of the Chloramine T/Oxidation buffer mixture was added and incubated for 5 min at room temperature. Following the completion of the reaction, 100 μL of the diluted p-dimethylaminobenzaldehyde (DMAB) reagent was added and incubated for 90 min at 60°C. The absorbance of each sample was measure at 560 nm, and hydroxyproline content was extrapolated from the standard curve using hydroxyproline standards.

Evaluation of therapeutic interactions

The therapeutic interactions between nintedanib and ADI were analyzed according to the method of Chou and Talalay[40] with the help of the CalcuSyn software suite (Biosoft, Cambridge, UK). CI values were determined by generating dose-response curves for various concentrations of nintedanib (0.625−4 μM) treatment in conjunction with ADI (0.625−4 μg/mL) and then calculated at different drug concentrations. According to Chou and Talalay,[40] a CI of <1 indicates a synergistic interaction, a CI of 1 indicates an additive interaction, and a CI of >1 indicates an antagonistic interaction.

Statistical analysis

Data derived from at least three independent experiments are represented as mean ± SE. Quantitative variables were assessed using an unpaired two-tailed Student's t test. Statistical differences in patient characteristics between the high-expression and low-expression groups were analyzed using a Fisher's exact test or Pearson chi-square test. All analyses were performed using SPSS software (version [v.] 20.0; SPSS, Chicago, IL, USA). All statistical tests were two sided, and p values < 0.05 were considered statistically significant.

SUPPLEMENTAL INFORMATION

Supplemental Information can be found online at https://doi.org/10.1016/j.ymthe.2021.01.028.

ACKNOWLEDGMENTS

The authors thank Dr. Richart Harper and Ms. Elena E. Foster (Department of Internal Medicine, UC Davis) for collection of lung tissue samples; Dr. Ssu-Wei Hsu (Integrative Pathobiology, UC Davis) and Ms. Wen-Hsin Chang (Institute of Molecular Medicine, College of Medicine, National Taiwan University) for bioinformatics and statistical support; Ms. Lisa Franzi, Dr. Szu-Jung Chen, Ms. Shenwen Gu, and Ms. Linhui Li (Department of Internal Medicine, UC Davis) for assistance with the animal experiments; as well as the UC Davis Comprehensive Cancer Center Biorepository for pathology support.

This work was supported by the California UCOP grants Tobacco-Related Disease Research Program (TRDRP 27KT-0004 and 28IR-0061), the NIH grants (NHLBI R01HL146802, 1K23HL138190, and T32 HL007013), and the DoD PRMRP grant W81XWH2110086 (#PR202411).

AUTHOR CONTRIBUTIONS

Conception and design, J.-M.L. and C.-H.C.; development of methodology, J.-M.L., D.C.Y., and C.-H.C.; acquisition of data (provided animals, acquired and managed patients, provided facilities, etc.), J.-M.L., D.C.Y., J.O., A.L., J.Z., N.J.K., and C.-H.C.; analysis and interpretation of data (e.g., statistical analysis, biostatistics, computational analysis), J.-M.L., D.C.Y., A.L., J.Z., and C.-H.C.; writing, review, and/or revision of the manuscript, J.-M.L., D.C.Y., J.L., and C.-H.C.; administrative, technical, or material support (i.e., reporting or organizing data, constructing databases), J.O., N.J.K., and C.-H.C.; study supervision, C.-H.C.

DECLARATION OF INTERESTS

The authors declare no competing interests.

REFERENCES

1. Ley, B., Collard, H.R., and King, T.E., Jr. (2011). Clinical course and prediction of survival in idiopathic pulmonary fibrosis. Am. J. Respir. Crit. Care Med. *183*, 431–440.
2. Martinez, F.J., Collard, H.R., Pardo, A., Raghu, G., Richeldi, L., Selman, M., Swigris, J.J., Taniguchi, H., and Wells, A.U. (2017). Idiopathic pulmonary fibrosis. Nat. Rev. Dis. Primers *3*, 17074.
3. Nalysnyk, L., Cid-Ruzafa, J., Rotella, P., and Esser, D. (2012). Incidence and prevalence of idiopathic pulmonary fibrosis: review of the literature. Eur. Respir. Rev. *21*, 355–361.
4. Myllärniemi, M., and Kaarteenaho, R. (2015). Pharmacological treatment of idiopathic pulmonary fibrosis - preclinical and clinical studies of pirfenidone, nintedanib, and N-acetylcysteine. Eur. Clin. Respir. J. *2*, https://doi.org/10.3402/ecrj.v2.26385.
5. Wollin, L., Wex, E., Pautsch, A., Schnapp, G., Hostettler, K.E., Stowasser, S., and Kolb, M. (2015). Mode of action of nintedanib in the treatment of idiopathic pulmonary fibrosis. Eur. Respir. J. *45*, 1434–1445.
6. Wollin, L., Maillet, I., Quesniaux, V., Holweg, A., and Ryffel, B. (2014). Antifibrotic and anti-inflammatory activity of the tyrosine kinase inhibitor nintedanib in experimental models of lung fibrosis. J. Pharmacol. Exp. Ther. *349*, 209–220.
7. Rangarajan, S., Locy, M.L., Luckhardt, T.R., and Thannickal, V.J. (2016). Targeted Therapy for Idiopathic Pulmonary Fibrosis: Where To Now? Drugs *76*, 291–300.
8. Dimitroulis, I.A. (2014). Nintedanib: a novel therapeutic approach for idiopathic pulmonary fibrosis. Respir. Care *59*, 1450–1455.
9. Richeldi, L. (2014). Treatments for idiopathic pulmonary fibrosis. N. Engl. J. Med. *371*, 783.
10. King, T.E., Jr., Noble, P.W., and Bradford, W.Z. (2014). Treatments for idiopathic pulmonary fibrosis. N. Engl. J. Med. *371*, 783–784.
11. Sanders, Y.Y., Kumbla, P., and Hagood, J.S. (2007). Enhanced myofibroblastic differentiation and survival in Thy-1(-) lung fibroblasts. Am. J. Respir. Cell Mol. Biol. *36*, 226–235.
12. Jordana, M., Schulman, J., McSharry, C., Irving, L.B., Newhouse, M.T., Jordana, G., and Gauldie, J. (1988). Heterogeneous proliferative characteristics of human adult lung fibroblast lines and clonally derived fibroblasts from control and fibrotic tissue. Am. Rev. Respir. Dis. *137*, 579–584.
13. Panganiban, R.A., and Day, R.M. (2011). Hepatocyte growth factor in lung repair and pulmonary fibrosis. Acta Pharmacol. Sin. *32*, 12–20.
14. Bjoraker, J.A., Ryu, J.H., Edwin, M.K., Myers, J.L., Tazelaar, H.D., Schroeder, D.R., and Offord, K.P. (1998). Prognostic significance of histopathologic subsets in idiopathic pulmonary fibrosis. Am. J. Respir. Crit. Care Med. *157*, 199–203.
15. Grimminger, F., Günther, A., and Vancheri, C. (2015). The role of tyrosine kinases in the pathogenesis of idiopathic pulmonary fibrosis. Eur. Respir. J. *45*, 1426–1433.
16. Wilson, C.L., and Hung, C.F. (2019). Another Weapon in the Battle against Idiopathic Pulmonary Fibrosis? Am. J. Respir. Cell Mol. Biol. *60*, 386–387.
17. Stella, G.M., Gentile, A., Balderacchi, A., Meloni, F., Milan, M., and Benvenuti, S. (2016). Ockham's razor for the MET-driven invasive growth linking idiopathic pulmonary fibrosis and cancer. J. Transl. Med. *14*, 256.
18. Garajová, I., Giovannetti, E., Biasco, G., and Peters, G.J. (2015). c-Met as a Target for Personalized Therapy. Transl. Oncogenomics *7* (*Suppl 1*), 13–31.
19. Para, R., Romero, F., George, G., and Summer, R. (2019). Metabolic Reprogramming as a Driver of Fibroblast Activation in PulmonaryFibrosis. Am. J. Med. Sci. *357*, 394–398.
20. Zhao, H., Dennery, P.A., and Yao, H. (2018). Metabolic reprogramming in the pathogenesis of chronic lung diseases, including BPD, COPD, and pulmonary fibrosis. Am. J. Physiol. Lung Cell. Mol. Physiol. *314*, L544–L554.
21. Zhao, Y.D., Yin, L., Archer, S., Lu, C., Zhao, G., Yao, Y., Wu, L., Hsin, M., Waddell, T.K., Keshavjee, S., et al. (2017). Metabolic heterogeneity of idiopathic pulmonary fibrosis: a metabolomic study. BMJ Open Respir. Res. *4*, e000183.
22. Kang, Y.P., Lee, S.B., Lee, J.M., Kim, H.M., Hong, J.Y., Lee, W.J., Choi, C.W., Shin, H.K., Kim, D.J., Koh, E.S., et al. (2016). Metabolic Profiling Regarding Pathogenesis of Idiopathic Pulmonary Fibrosis. J. Proteome Res. *15*, 1717–1724.
23. Wang, X.M., Zhang, Y., Kim, H.P., Zhou, Z., Feghali-Bostwick, C.A., Liu, F., Ifedigbo, E., Xu, X., Oury, T.D., Kaminski, N., and Choi, A.M. (2006). Caveolin-1: a critical regulator of lung fibrosis in idiopathic pulmonary fibrosis. J. Exp. Med. *203*, 2895–2906.
24. Keshet, R., Szlosarek, P., Carracedo, A., and Erez, A. (2018). Rewiring urea cycle metabolism in cancer to support anabolism. Nat. Rev. Cancer *18*, 634–645.
25. Trott, J.F., Hwang, V.J., Ishimaru, T., Chmiel, K.J., Zhou, J.X., Shim, K., Stewart, B.J., Mahjoub, M.R., Jen, K.Y., Barupal, D.K., et al. (2018). Arginine reprogramming in ADPKD results in arginine-dependent cystogenesis. Am. J. Physiol. Renal Physiol. *315*, F1855–F1868.
26. Patil, M.D., Bhaumik, J., Babykutty, S., Banerjee, U.C., and Fukumura, D. (2016). Arginine dependence of tumor cells: targeting a chink in cancer's armor. Oncogene *35*, 4957–4972.
27. Delage, B., Fennell, D.A., Nicholson, L., McNeish, I., Lemoine, N.R., Crook, T., and Szlosarek, P.W. (2010). Arginine deprivation and argininosuccinate synthetase expression in the treatment of cancer. Int. J. Cancer *126*, 2762–2772.
28. Yang, D.C., Li, J.M., Xu, J., Oldham, J., Phan, S.H., Last, J.A., Wu, R., and Chen, C.H. (2019). Tackling MARCKS-PIP3 circuit attenuates fibroblast activation and fibrosis progression. FASEB J. *33*, 14354–14369.
29. Zou, S., Wang, X., Liu, P., Ke, C., and Xu, S. (2019). Arginine metabolism and deprivation in cancer therapy. Biomed. Pharmacother. *118*, 109210.
30. Liang, J., Liu, N., Liu, X., Mena, J.M., Xie, T., Geng, Y., Huan, C., Zhang, Y., Taghavifar, F., Huang, G., et al. (2019). Mitogen-activated Protein Kinase-activated Protein Kinase 2 Inhibition Attenuates Fibroblast Invasion and Severe Lung Fibrosis. Am. J. Respir. Cell Mol. Biol. *60*, 41–48.
31. Li, Y., Jiang, D., Liang, J., Meltzer, E.B., Gray, A., Miura, R., Wogensen, L., Yamaguchi, Y., and Noble, P.W. (2011). Severe lung fibrosis requires an invasive fibroblast phenotype regulated by hyaluronan and CD44. J. Exp. Med. *208*, 1459–1471.
32. Pierce, E.M., Carpenter, K., Jakubzick, C., Kunkel, S.L., Flaherty, K.R., Martinez, F.J., and Hogaboam, C.M. (2007). Therapeutic targeting of CC ligand 21 or CC chemokine receptor 7 abrogates pulmonary fibrosis induced by the adoptive transfer of human pulmonary fibroblasts to immunodeficient mice. Am. J. Pathol. *170*, 1152–1164.
33. Chen, C.H., Thai, P., Yoneda, K., Adler, K.B., Yang, P.C., and Wu, R. (2014). A peptide that inhibits function of Myristoylated Alanine-Rich C Kinase Substrate (MARCKS) reduces lung cancer metastasis. Oncogene *33*, 3696–3706.
34. Chen, C.H., Statt, S., Chiu, C.L., Thai, P., Arif, M., Adler, K.B., and Wu, R. (2014). Targeting myristoylated alanine-rich C kinase substrate phosphorylation site domain

in lung cancer. Mechanisms and therapeutic implications. Am. J. Respir. Crit. Care Med. *190*, 1127–1138.

35. Cheng, C.T., Qi, Y., Wang, Y.C., Chi, K.K., Chung, Y., Ouyang, C., Chen, Y.R., Oh, M.E., Sheng, X., Tang, Y., et al. (2018). Arginine starvation kills tumor cells through aspartate exhaustion and mitochondrial dysfunction. Commun. Biol. *1*, 178.
36. Szlosarek, P.W., Klabatsa, A., Pallaska, A., Sheaff, M., Smith, P., Crook, T., Grimshaw, M.J., Steele, J.P., Rudd, R.M., Balkwill, F.R., and Fennell, D.A. (2006). In vivo loss of expression of argininosuccinate synthetase in malignant pleural mesothelioma is a biomarker for susceptibility to arginine depletion. Clin. Cancer Res. *12*, 7126–7131.
37. Przystal, J.M., Hajji, N., Khozoie, C., Renziehausen, A., Zeng, Q., Abaitua, F., Hajitou, A., Suwan, K., Want, E., Bomalaski, J., et al. (2018). Efficacy of arginine depletion by ADI-PEG20 in an intracranial model of GBM. Cell Death Dis. *9*, 1192.
38. Changou, C.A., Chen, Y.R., Xing, L., Yen, Y., Chuang, F.Y., Cheng, R.H., Bold, R.J., Ann, D.K., and Kung, H.J. (2014). Arginine starvation-associated atypical cellular death involves mitochondrial dysfunction, nuclear DNA leakage, and chromatin autophagy. Proc. Natl. Acad. Sci. USA *111*, 14147–14152.
39. Riess, C., Shokraie, F., Classen, C.F., Kreikemeyer, B., Fiedler, T., Junghanss, C., and Maletzki, C. (2018). Arginine-Depleting Enzymes - An Increasingly Recognized Treatment Strategy for Therapy-Refractory Malignancies. Cell. Physiol. Biochem. *51*, 854–870.
40. Chou, T.C., and Talalay, P. (1984). Quantitative analysis of dose-effect relationships: the combined effects of multiple drugs or enzyme inhibitors. Adv. Enzyme Regul. *22*, 27–55.
41. Liu, G., and Summer, R. (2019). Cellular Metabolism in Lung Health and Disease. Annu. Rev. Physiol. *81*, 403–428.
42. Zhang, Y., and Kaminski, N. (2012). Biomarkers in idiopathic pulmonary fibrosis. Curr. Opin. Pulm. Med. *18*, 441–446.
43. Miyamoto, T., Lo, P.H.Y., Saichi, N., Ueda, K., Hirata, M., Tanikawa, C., and Matsuda, K. (2017). Argininosuccinate synthase 1 is an intrinsic Akt repressor transactivated by p53. Sci. Adv. *3*, e1603204.
44. Huang, H.Y., Wu, W.R., Wang, Y.H., Wang, J.W., Fang, F.M., Tsai, J.W., Li, S.H., Hung, H.C., Yu, S.C., Lan, J., et al. (2013). ASS1 as a novel tumor suppressor gene in myxofibrosarcomas: aberrant loss via epigenetic DNA methylation confers aggressive phenotypes, negative prognostic impact, and therapeutic relevance. Clin. Cancer Res. *19*, 2861–2872.
45. Ding, X., Ji, J., Jiang, J., Cai, Q., Wang, C., Shi, M., Yu, Y., Zhu, Z., and Zhang, J. (2018). HGF-mediated crosstalk between cancer-associated fibroblasts and MET-unamplified gastric cancer cells activates coordinated tumorigenesis and metastasis. Cell Death Dis. *9*, 867.
46. Kendall, R.T., and Feghali-Bostwick, C.A. (2014). Fibroblasts in fibrosis: novel roles and mediators. Front. Pharmacol. *5*, 123.
47. Nakerakanti, S., and Trojanowska, M. (2012). The Role of TGF-β Receptors in Fibrosis. Open Rheumatol. J. *6*, 156–162.
48. Puccini, A., Marín-Ramos, N.I., Bergamo, F., Schirripa, M., Lonardi, S., Lenz, H.J., Loupakis, F., and Battaglin, F. (2019). Safety and Tolerability of c-MET Inhibitors in Cancer. Drug Saf. *42*, 211–233.
49. Iyer, S.N., Hyde, D.M., and Giri, S.N. (2000). Anti-inflammatory effect of pirfenidone in the bleomycin-hamster model of lung inflammation. Inflammation *24*, 477–491.
50. Maarsingh, H., Pera, T., and Meurs, H. (2008). Arginase and pulmonary diseases. Naunyn Schmiedebergs Arch. Pharmacol. *378*, 171–184.
51. Gao, L., Zhang, J.H., Chen, X.X., Ren, H.L., Feng, X.L., Wang, J.L., and Xiao, J.H. (2019). Combination of L-Arginine and L-Norvaline protects against pulmonary fibrosis progression induced by bleomycin in mice. Biomed. Pharmacother. *113*, 108768.
52. Chen, C.H., Cheng, C.T., Yuan, Y., Zhai, J., Arif, M., Fong, L.W., Wu, R., and Ann, D.K. (2015). Elevated MARCKS phosphorylation contributes to unresponsiveness of breast cancer to paclitaxel treatment. Oncotarget *6*, 15194–15208.
53. Chen, C.H., Chiu, C.L., Adler, K.B., and Wu, R. (2014). A novel predictor of cancer malignancy: up-regulation of myristoylated alanine-rich C kinase substrate phosphorylation in lung cancer. Am. J. Respir. Crit. Care Med. *189*, 1002–1004.
54. Chen, C.H., Chang, W.H., Su, K.Y., Ku, W.H., Chang, G.C., Hong, Q.S., Hsiao, Y.J., Chen, H.C., Chen, H.Y., Wu, R., et al. (2016). HLJ1 is an endogenous Src inhibitor suppressing cancer progression through dual mechanisms. Oncogene *35*, 5674–5685.
55. Chen, C.H., Chuang, S.M., Yang, M.F., Liao, J.W., Yu, S.L., and Chen, J.J. (2012). A novel function of YWHAZ/β-catenin axis in promoting epithelial-mesenchymal transition and lung cancer metastasis. Mol. Cancer Res. *10*, 1319–1331.
56. Limjunyawong, N., Mitzner, W., and Horton, M.R. (2014). A mouse model of chronic idiopathic pulmonary fibrosis. Physiol. Rep. *2*, e00249.